ADVANCED REVIEW

WIREs NANOMEDICINE AND NANOBIOTECHNOLOGY WILEY

Clinical magnetic hyperthermia requires integrated magnetic particle imaging

Sean Healy[1,2] | Andris F. Bakuzis[3] | Patrick W. Goodwill[4] |
Anilchandra Attaluri[5] | Jeff W. M. Bulte[1,6,7,8,9] | Robert Ivkov[2,9,10,11]

[1]Department of Biomedical Engineering, Whiting School of Engineering, Johns Hopkins University, Baltimore, Maryland, USA

[2]Department of Radiation Oncology and Molecular Radiation Sciences, Johns Hopkins University School of Medicine, Baltimore, Maryland, USA

[3]Instituto de Física and CNanoMed, Universidade Federal de Goiás, Goiânia, GO, Brazil

[4]Magnetic Insight, Inc., Alameda, California, USA

[5]Department of Mechanical Engineering, Pennsylvania State University, Harrisburg, Harrisburg, Pennsylvania, USA

[6]Russell H. Morgan Department of Radiology and Radiological Science, Johns Hopkins Hospital, Baltimore, Maryland, USA

[7]Cellular Imaging Section and Vascular Biology Program, Institute for Cell Engineering, Johns Hopkins University School of Medicine, Baltimore, Maryland, USA

[8]Department of Chemical and Biomolecular Engineering, Whiting School of Engineering, Johns Hopkins University, Baltimore, Maryland, USA

[9]Department of Oncology, Johns Hopkins University School of Medicine, Baltimore, Maryland, USA

[10]Department of Materials Science and Engineering, Whiting School of Engineering, Johns Hopkins University, Baltimore, Maryland, USA

[11]Department of Mechanical Engineering, Whiting School of Engineering, Johns Hopkins University, Baltimore, Maryland, USA

Correspondence
Robert Ivkov, Department of Radiation Oncology and Molecular Radiation Sciences, Johns Hopkins University School of Medicine, David H. Koch Cancer Research Building, Room 442, 1550 Orleans Street, Baltimore, MD 21231, USA.
Email: rivkov1@jhmi.edu

Abstract

Magnetic nanomaterials that respond to clinical magnetic devices have significant potential as cancer nanotheranostics. The complexities of their physics, however, introduce challenges for these applications. Hyperthermia is a heat-based cancer therapy that improves treatment outcomes and patient survival when controlled energy delivery is combined with accurate thermometry. To date, few technologies have achieved the needed evolution for the demands of the clinic. Magnetic fluid hyperthermia (MFH) offers this potential, but to be successful it requires particle-imaging technology that provides real-time thermometry. Presently, the only technology having the potential to meet these requirements is magnetic particle imaging (MPI), for which a proof-of-principle demonstration with MFH has been achieved. Successful clinical translation and adoption of integrated MPI/MFH technology will depend on successful resolution of the technological challenges discussed.

This article is categorized under:

Therapeutic Approaches and Drug Discovery > Nanomedicine for Oncologic Disease

Diagnostic Tools > In Vivo Nanodiagnostics and Imaging

1 | INTRODUCTION

Magnetic nanoparticles that are responsive to clinical magnetic fields offer multi-modal nanomedicine capabilities. For combined diagnostic and therapeutic, that is, *theranostic* applications, the physical and magnetic properties of magnetic nanoparticles must be matched with the device used to activate them (Cole et al., 2011; Dennis et al., 2015; Dennis & Ivkov, 2013; Gul et al., 2019). Though many types of magnetic nanoparticles exist, most research focuses on magnetic iron oxides, that is, magnetite (Fe_3O_4) or maghemite (γ-Fe_2O_3), as iron oxide is the only magnetic nanomaterial approved for use in humans. With continuous clinical use for nearly one century, iron oxide's general biocompatibility and clinical utility is established, though a detailed understanding of their complex interactions with biological systems continues to evolve (Korangath et al., 2020; Soetaert et al., 2020; Toraya et al., 2012; Zanganeh et al., 2016). Since the 1980s, various magnetic iron oxide nanoparticle (MIONP) formulations have been used as clinical contrast agents for magnetic resonance imaging (MRI) (Bulte & Daldrup-Link, 2018; Bulte & Kraitchman, 2004). Magnetic fluid hyperthermia (MFH) with MIONPs was clinically approved in 2010 for treating recurrent glioblastoma with radiation following demonstrations of improved overall survival in clinical trials (Maier-Hauff et al., 2007, 2011; Marchal et al., 2015). Thus, MIONPs have theranostic potential because they simultaneously can be agents for (magnetic) diagnostic imaging and (magnetically activated) hyperthermia therapy. Yet, no MIONP formulation approved for *both* diagnostic imaging and cancer therapy is available; and, there is no clinical device approved for *combined* imaging and therapy with MIONPs. We focus on requirements of MIONPs and device(s) that, given a review of literature, are most likely to translate successfully to clinical cancer theranostics.

2 | BENEFITS AND CHALLENGES OF HYPERTHERMIA AS CANCER THERAPY

Hyperthermia is a heat-based cancer therapy having the objective to raise local tissue temperature to kill cancer cells or to sensitize them to other treatments (Falk & Issels, 2001). Therapeutic effectiveness of hyperthermia depends on thermal dose, defined as time-at-temperature. Treatment temperatures are typically 41–46°C, and treatment times range between ~30 and ~60 min to conform to individual patient needs and to accommodate clinical workflow (Dewhirst et al., 2011, 2021; Sapareto & Dewey, 1984). Temperatures exceeding 47°C produce thermal ablation, and treatment at temperatures 39–41°C produces mild hyperthermia that is generally not directly cytocidal but enhances effectiveness of DNA-damaging agents such as radiation and some chemotherapies. The clinical benefits of hyperthermia stem from its ability to disrupt or abrogate DNA-damage repair, reverse tumor hypoxia, increase cellular metabolic rate, and induce other physiologic changes (Dewhirst et al., 2012, 2021). Recent evidence suggests additional benefits of hyperthermia include induction of anti-tumor immune responses by various mechanisms, particularly when tumors are small (Chao et al., 2019; Oei et al., 2019; Repasky et al., 2013; Toraya-Brown & Fiering, 2014).

TABLE 1 Selection of key phase III clinical hyperthermia studies and recent updates

| Reference | Tumor type | Number of patients | | | End points | | |
		N	Ctrl	+HT	Ctrl	Tx (Ctrl + HT)	p
van der Zee et al. (2000)	Bladder, cervix, or rectum	358	(RT) 176	182	39% CR (3 months) 24% OS (all; 3 years)	55% CR (3 months) 30% OS (all; 3 years)	<0.001
	Cervix only				57% CR (3 months)	83% CR (3 months)	0.003
					27% OS (3 years)	51% OS (3 years)	0.009
Sneed et al. (1998)	Glioblastoma (brain) (after RT)	68	(RT + BR) 33	35	15% OS (2 years)	31% OS (2 years)	0.02
Overgaard et al. (1995)	Melanoma	68	(RT) 65	63	28% LC (2 years)	46% LC (2 years)	0.008
Datta et al. (1990)	Head and neck	65	(RT) 32	33	31% CR (8 weeks)	55% CR (8 weeks)	
Harima et al. (2009)	Cervix	40	(RT + BR) 20	20	50% CR	80% CR	0.048
					48.5% LRFS (3 years)	79.7% LRFS (3 years)	0.048
Wang et al. (2020)	Cervix	373	(CRT) 191	182	81.9% OS (5 years)	72.3% OS (5 years)	0.04

Abbreviations: BR, brachytherapy; CR, complete response; CRT, chemoradiotherapy; LC, local control; LRFS, local relapse-free survival; OS, overall survival; RT, external beam radiotherapy.

Cancer patients benefit most from hyperthermia if spatiotemporal control of thermal energy is precise, and if concomitant dosimetry (i.e., thermometry) assures treatments are reproducible and conform to a prescribed plan (Dewhirst et al., 2011, 2012, 2021). Indeed, evidence suggests that poorly executed or improperly combined thermal treatments can aggravate disease by promoting tumorigenesis and metastatic dissemination (Markezana et al., 2021; Oda et al., 1985; Oei et al., 2019; Thrall et al., 1996; Yerushalmi, 1976). Technological challenges encountered with energy delivery and control, and thermometry are largely responsible for historically lagging clinical adoption of hyperthermia. Further contributing to slow adoption has been the complexity of older systems, and the lack of sufficient clinical data correlating precise temperature–time dose escalation with response (Crezee et al., 2015; Dewhirst et al., 2021; Kok et al., 2020). Recent engineering advances have, however, produced a number of systems from which a growing body of data demonstrates the benefits of combined therapy with hyperthermia (Table 1) (Dewhirst et al., 2021; Fiorentini et al., 2020; Kok et al., 2020). Individual patient benefits depend on individual conditions; and, a growing consensus acknowledges disease response to treatment and overall survival improve when *quality* hyperthermia is combined with a standard-of-care treatment (Dewhirst et al., 2021; Issels et al., 2016). Consequently, hyperthermia is approved for use in many countries with ionizing radiation to treat recurrent tumors, particularly in a re-irradiation setting (Crezee et al., 2015). Addition of hyperthermia to chemoradiotherapy regimens, an increasingly common practice in standard-of-care for many solid tumors, offers potentially more clinical impact to further extend overall survival (Table 1; Dewhirst et al., 2021; Fiorentini et al., 2020).

3 | MFH: THE FIRST THERMAL NANOMEDICINE

Of the approved and clinically validated hyperthermia modalities, MFH, also called magnetic nanoparticle hyperthermia, is the only thermal cancer nanomedicine that provides unique advantages arising directly from the nanoparticles (Soetaert et al., 2020). Currently, MFH involves intratumor delivery of MIONPs and application of an alternating magnetic field (AMF) to generate local non-ablative heating via magnetic hysteresis loss (Figure 1; Section 10) (Dennis & Ivkov, 2013; Ivkov, 2013). Originally proposed in 1957 by Gilchrist et al. (Gilchrist et al., 1957), a substantial research and preclinical effort led to eventual clinical validation of MFH for glioblastoma (Jordan et al., 2006; Maier-Hauff et al., 2007, 2011; Marchal et al., 2015). Other human clinical trials demonstrated benefits of MFH for prostate cancer showing its relevance to treat other cancers (Johannsen et al., 2005, 2010; Johannsen, Gneveckow, Taymoorian, et al., 2007; Johannsen, Gneveckow, Thiesen, et al., 2007). To date though, only one nanoparticle-based thermal therapy product, NanoTherm®, is approved for treating cancer (Mahmoudi et al., 2018).

A key advantage offered by MFH over other hyperthermia modalities is that AMF adjustment controls the heat generated within the target. Being weakly diamagnetic, tissue does not attenuate magnetic fields thus non-invasive control
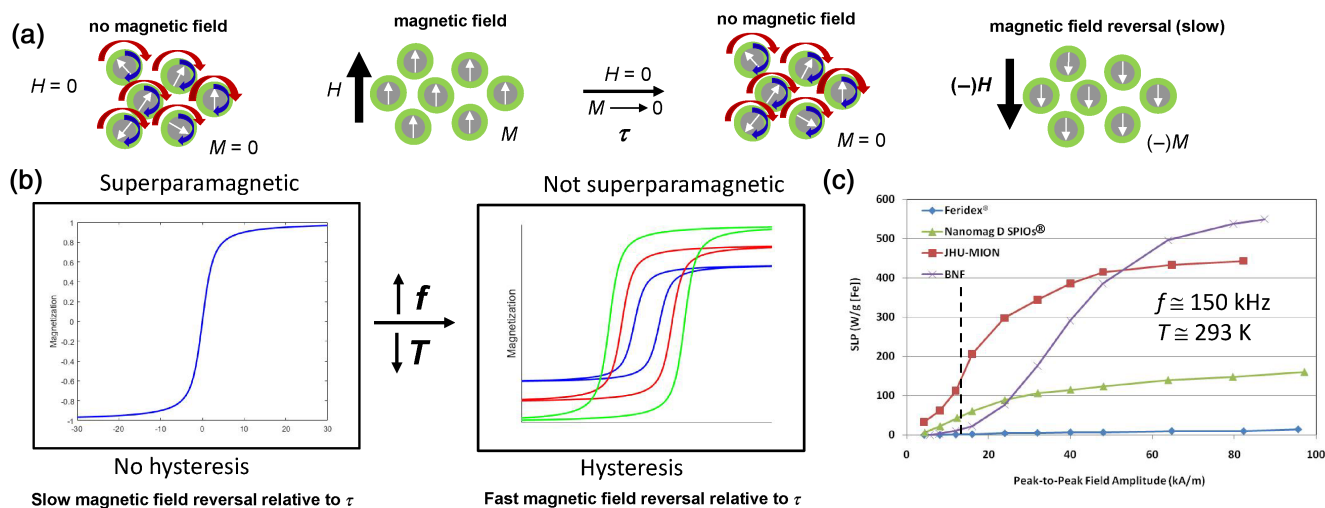
FIGURE 1 Magnetic iron oxide nanoparticles (MIONPs) exhibit unique behavior that can be exploited for hyperthermia. (a) A collection of freely suspended and non-interacting single-domain, spherical magnets are magnetically isotropic at $T = 310.15$ K (37°C) with zero measured moment ($M = 0$) with no magnetic field ($H = 0$) (far left). However, moments of the nanomagnets (white arrows) will align with the direction of an external field ($H > 0$), yielding a net magnetization ($M > 0$) (middle left). When the external field is removed, nanomagnet moments relax to isotropic condition, $M \to 0$, with a characteristic time scale τ, that is determined by inherent properties of the nanomagnets and experimental conditions. This is called *superparamagnetism* and occurs through a combination of internal moment reversal (Néel relaxation, blue arrows) and whole particle rotations (Brownian relaxation, red arrows) (middle right). Application of a magnetic field in the reverse direction aligns moments with the field (far right). (b) When a collection of freely suspended and non-interacting MIONPs is exposed to an external field that changes direction at a time scale slower than τ, MIONP moments align instantaneously with the field, yielding a magnetization that follows a *reversible* path mimicking superparamagnetism (left). With increasing magnetic field frequency f, or decreasing temperature T, individual moments lag causing the magnetization to trace an *irreversible* path, or hysteresis that signifies a transition out of the superparamagnetic regime. Magnetic hysteresis dissipates heat, proportional to the area of the hysteresis loop, with total heat produced by repeated and rapid cycling in an alternating magnetic field (AMF). (c) For clinical magnetic fluid hyperthermia (MFH), MIONPs must generate sufficient heat in an AMF within the clinical limits of f and H (dashed vertical line). Feridex®, a magnetic resonance imaging (MRI) MIONP contrast agent displays superparamagnetism (i.e., SPM MIONP, or SPION) at the test conditions, yielding negligible heating. The other MIONPs are not superparamagnets and generate heat at the test conditions, but display differing hysteresis responses to H. Magnetic moments of crystallites or particles can influence relaxation behavior of neighbors, influencing response of the system to external magnetic fields. This leads to *collective behavior* that can be used to tailor heating properties of magnetic nanoparticles for medical applications (see text). Data previously published in Bordelon et al. (2011) and Dennis et al. (2015) were used in the figure

of MFH deep within the patient is possible. The nanometer size of the MIONPs and their suspension in fluid offer patient-specific precision therapy, but only with accurate thermometry (Dewhirst et al., 2011, 2021; Gilchrist et al., 1957; Ivkov, 2013). Another requirement for prescriptive MFH is spatially precise imaging of MIONP in tissues to enable robust treatment plans.

4 | LIMITATIONS OF MFH

MFH is a powerful clinical technique supported by over six decades of research and clinical experience, but the current technology has the following limitations:

1. Limited information of MIONP distribution in tissue.
2. Limited spatial control of AMF.
3. Limited and invasive thermometry.

Current MFH only partially meets the demands of clinical hyperthermia. New technology must (1) integrate high-resolution (onboard) MIONP imaging with MFH for accurate image-guided therapeutic heating; (2) reduce off-target
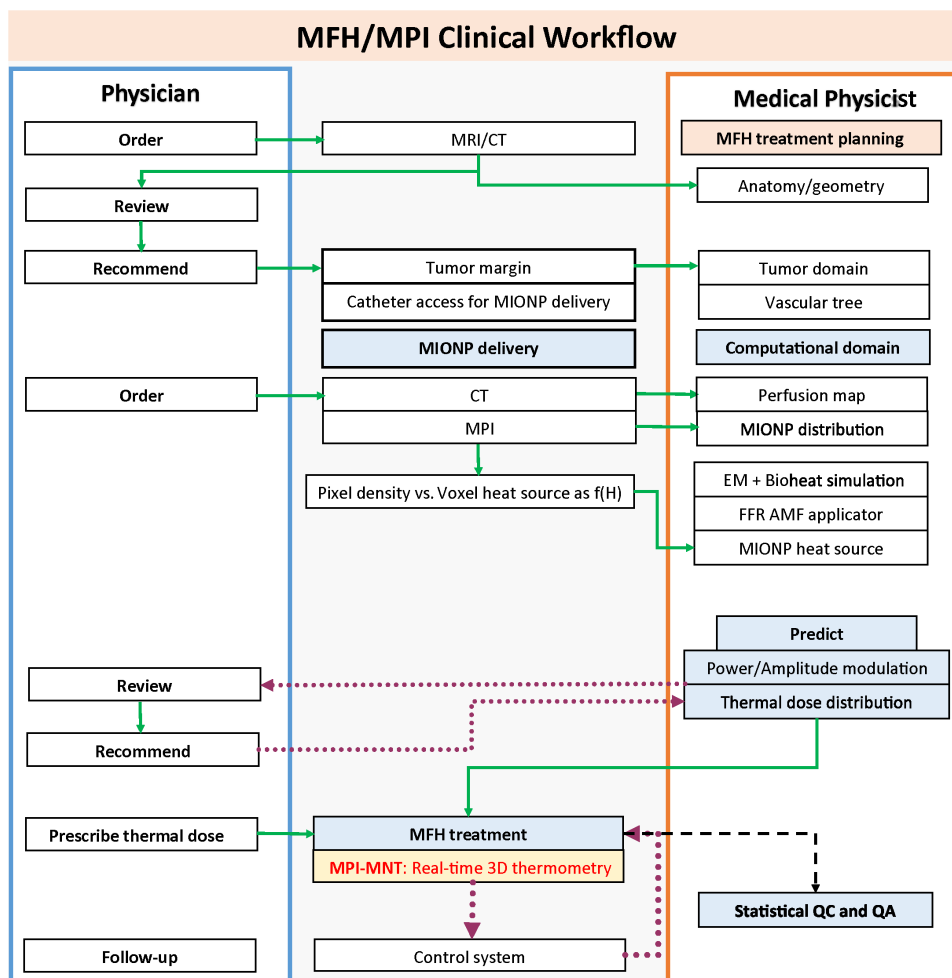
FIGURE 2 Block diagram of imaging-guided MFH clinical workflow that relies on an integrated MPI-MFH-MNT device. Future imaging-guided MFH would mimic clinical workflow used in modern radiation oncology to treat solid tumors with ionizing radiation. Separately, the device can provide diagnostic imaging with the same MIONPs used for therapy, and once disease is confirmed, anatomical imaging (CT and/or MRI) can be coregistered for treatment planning

tissue heating; and, (3) provide volumetric thermometry (Figures 2–4). Off-target heating occurs when MIONPs outside the target are activated (Kut et al., 2012; Yang et al., 2020), and from nonspecific AMF-induced heating of tissues due to eddy currents (Atkinson et al., 1984; Ivkov et al., 2005). Imaging and thermometry ensure quality of treatments for efficacy, while limiting off-target heating addresses patient safety. Heat is a potent agent that does not inherently target cancer, placing the burden on technology to control its delivery and distribution.

Magnetic particle imaging (MPI) is an evolving modality that uses the directionality of magnetic fields and time-dependent response(s) of "magnetized" MIONPs to image directly MIONPs in tissues (Figures 1 and 5, and Section 6) (Gleich & Weizenecker, 2005). The same physics that enables this direct visualization of MIONPs can also spatially confine tissue heating (Figure 5 and Section 7) and extract temperature data from the MIONPs because the time-dependent magnetization response(s) of MIONPs explicitly depend(s) on temperature (Figure 1 and Section 8). To fully exploit this potential, an integrated MPI-MFH device capable of magnetic nanoparticle thermometry (MNT) requires a combination of static (time invariant) and alternating (time varying) magnetic fields, with magnetic sensors ("pickup coils") strategically positioned around a sample stage or patient bed (Figure 5 and Section 9). In turn, the time-dependent magnetic responsiveness of the MIONPs must match the time-scale of the device (Section 10). As the imaging, heating, and thermometry now depend entirely on the MIONPs, or rather the magnetic properties of the MIONPs in tissue, clinical success or failure of this approach relies disproportionally on the subtleties of time-dependent relaxations of the MIONPs (Section 11).
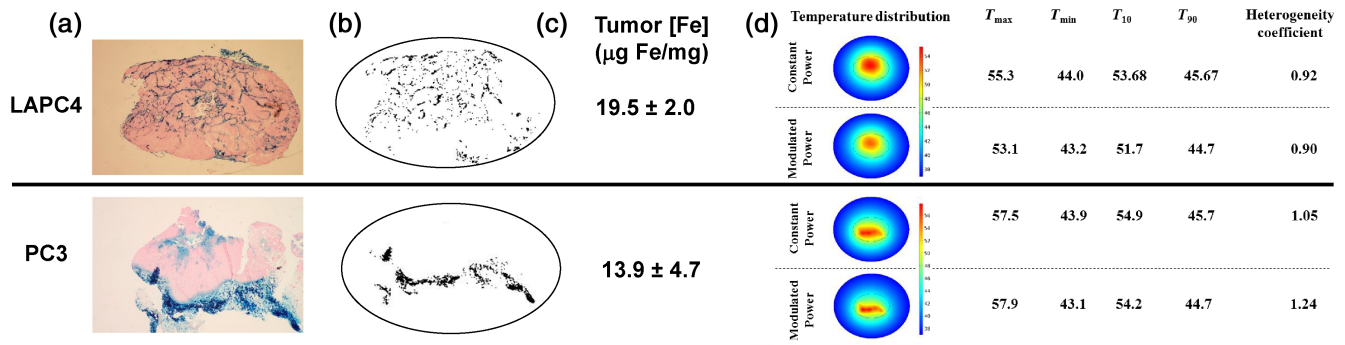
Figure 3, part (d) table:

	Temperature distribution	T_{max}	T_{min}	T_{10}	T_{90}	Heterogeneity coefficient
LAPC4 — Constant Power		55.3	44.0	53.68	45.67	0.92
LAPC4 — Modulated Power		53.1	43.2	51.7	44.7	0.90
PC3 — Constant Power		57.5	43.9	54.9	45.7	1.05
PC3 — Modulated Power		57.9	43.1	54.2	44.7	1.24

Tumor [Fe] (μg Fe/mg): LAPC4 = 19.5 ± 2.0; PC3 = 13.9 ± 4.7

FIGURE 3 MIONP intratumor distribution is unpredictable and heterogeneous, requiring direct imaging for MFH treatment planning. (a) Prussian blue-stained human prostate cancer (PC3 and LAPC4) tumor tissue xenografts grown in male nude mice (single sections) were used as models. Tumor volume was 0.15 ± 0.02 cm^3 and 5 mg Fe/cm^3 of tumor was directly injected into tumors (reprinted with permission from Attaluri et al., 2015). (b) Histology sections were digitized and images processed in MATLAB. (c) Fe recovered from tumors using ICP MS shows that the total concentration in tumors also varies. (d) Computed 2D temperature distributions using digitized MIONP distribution shows MFH with amplitude-modulated control reduces temperature heterogeneity when compared to constant power MFH. Images derived from MIONP distributions shown in (a) and (b). In LAPC4, MIONPs show relatively uniform distributions; whereas, in PC3 the MIONPs were concentrated along the major axis. Power modulation ameliorated the effects of MIONP heterogeneity by reducing the area of hot zone near high concentrations of MIONPs and reduced the temperature at the tumor-tissue boundary. T_{max} and T_{min} are the maximum and minimum temperatures inside the tumor, respectively. T_{10} and T_{90} are the temperatures achieved by at least 10% and 90% of the tumor area, respectively, with the dimensionless heterogeneity coefficient indicating the temperature heterogeneity relative to T_{90}, or temperature uniformity. Note that for the concentrated MIONPs in the PC3 tumor model, modulated power did not enhance temperature uniformity, but it reduced the area of ablation in the tumor, and reduced damage to normal tissue. Precise onboard imaging of MIONPs for each tumor with 3D distribution will improve MFH for precision therapy. Reprinted with permission from Kandala et al. (2019)
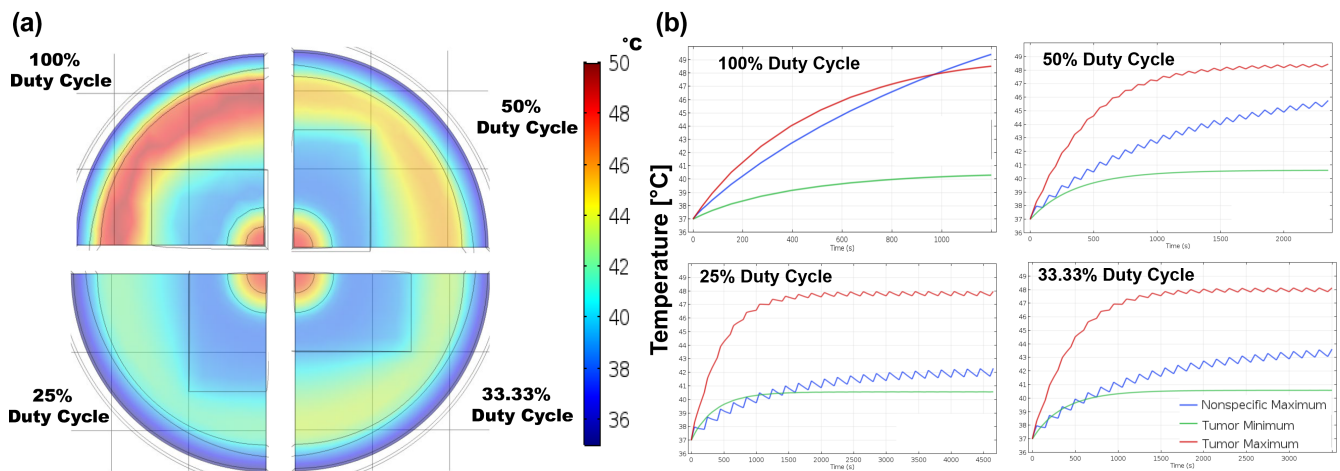

FIGURE 4 Pulsed AMF during MFH provides an effective means to manage/reduce adverse effects of off-target induced-eddy current heating in tissues. (a) Pulsing power and reducing duty cycle (ratio of working time to total time, where 100% is continuous power) enables physiological thermoregulatory cooling to effectively dissipate heat during power OFF cycles. Shown are simulated temperature distributions for 100%, 50%, 33.3%, and 25% duty cycles in a human scale computational model after 20 min of MIONP treatment. MIONPs are in the center of the circular diagram. (b) Simulated temperature rise for 100%, 50%, 33.3%, and 25% duty cycles in human scale computational models during MFH treatment demonstrate that by increasing treatment time, MIONP heating achieves similar temperatures in the tumor target. Note the change in the time scale on x-axis. Reprinted with permission from Attaluri, Kandala, et al. (2020)

Thus, time-dependent (magnetic) responses of MIONPs to external time-varying magnetic fields simultaneously present us with their greatest advantage *and* their greatest challenge for clinical MFH. MIONP size polydispersity and their uncontrolled/unpredictable colloidal state in biological tissues are perhaps the most significant challenges encountered for translation from laboratory to clinic. Methods to manufacture MIONPs at a scale needed to support clinical use
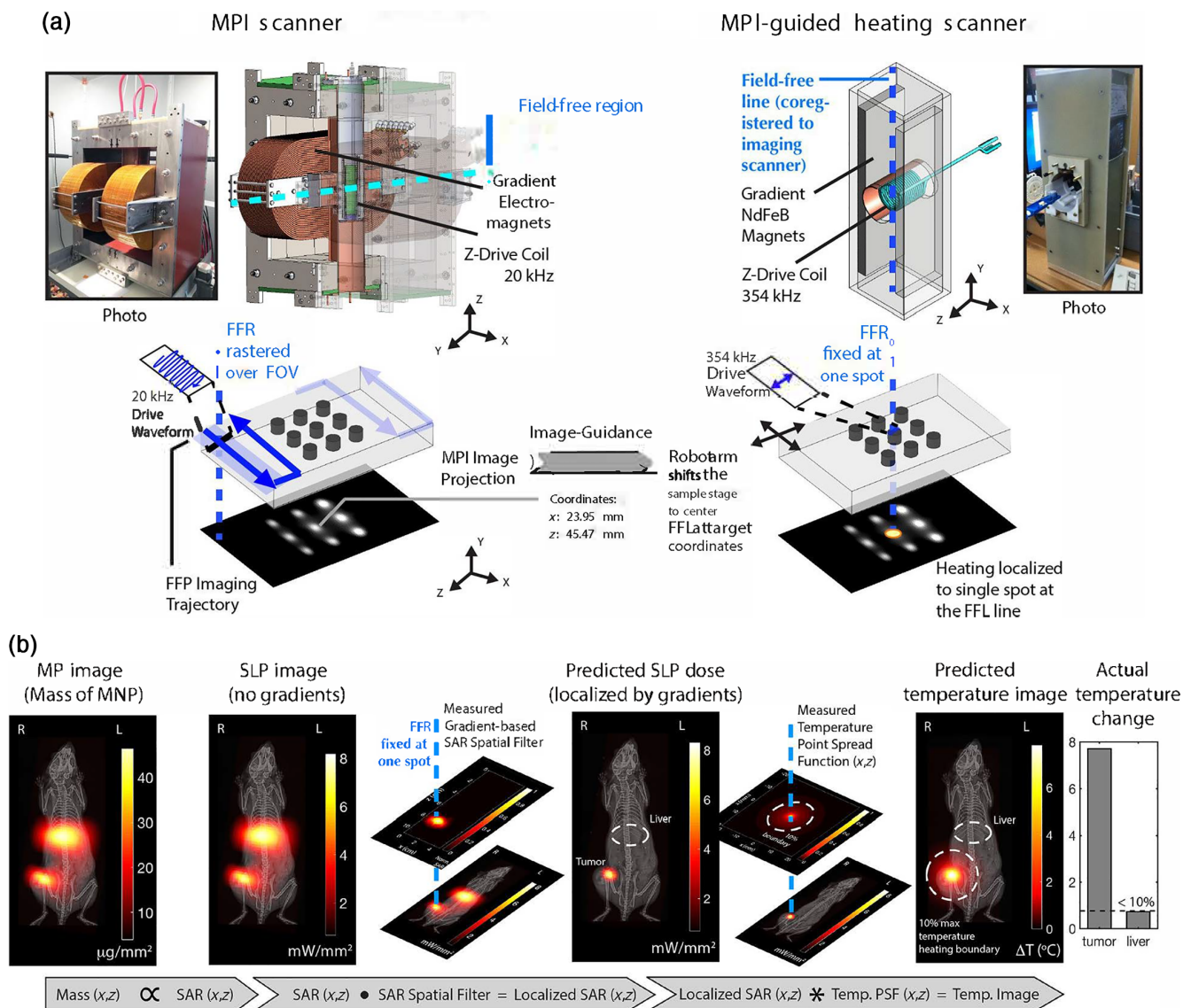
FIGURE 5 A proof-of-concept MPI integration with MFH demonstration. (a) Hardware setup for MPI scanner and image-guided MPI/MFH. (Left) MPI scanner. To obtain an image, the sensitive field-free-region (FFR) is rastered through a volume. In this example, a field-free-line (FFL) geometry was used, and images obtained are similar to projection scintigraphy. (Top right) MFH with MPI. A separate higher-frequency MPI/MFH scanner with the same FFL geometry was used for application of MFH. For image-guided therapy, coordinates were matched between the two scanners such that the imaging information from the first scanner was used to define MFH therapeutic trajectories in the MPI/MFH system. The user was able to select a target from the MPI image, and the corresponding coordinates on the image was sent to the MPI/MFH heating scanner. The robot arm shifted the co-registered animal bed to center the FFL of the heating scanner to the requested coordinates. To locally heat only the target, the FFL was held in place over the target while a higher frequency (354 kHz) AMF excitation field was applied. (b) Designing a heating "prescription" using MPI/MFH integrated scanner and a forward model to predict the temperature distribution from the MPI data of the MIONP biodistribution. To predict the localization effect of the MPI gradients, the gradient-less SAR (or SLP) image with the known suppression effect of the MPI gradients (SAR filter) with FFR centered at the therapeutic target can be used. A prediction of the SAR/SLP dose after gradient localization, which can be integrated into the heat transfer modeling to calculate CEM43. To account for heat transfer, the previous image would be convolved with a temperature spatial point spread function (PSF). Reproduced with permission from Tay et al. (2018)

($\geq 10^2$ kg/year) invariably produces nanoparticles having a range of volumes, or polydispersity of size. As the volume of the iron oxide nanocrystallite(s) comprising a MIONP explicitly influences its magnetic properties (Sections 10 and 11), the degree of polydispersity inevitably plays a role in clinical performance. When introduced into biological tissues, either directly by percutaneous delivery or systemically by intravenous/intra-arterial infusion, MIONP distribution is

heterogeneous and their physical motion restricted. Concentrated aggregates of MIONPs (i.e., reduced interparticle distance) as found in a tumor often display substantially different magnetic responsiveness than their freely suspended counterparts, whose properties often determine their initial suitability for clinical application. This disconnect is both unavoidable and unaddressed either by clinically relevant physical models or physical characterization methods. Furthermore, efforts to develop "pristine" and *nearly* monodisperse MIONPs are likely futile as any advantages are likely overwhelmed by the effects of aggregation in tissue. The electromagnetic force is long-range (explicitly, infinite) thus creating the potential for profound internal (*intraparticle*) and external (*interparticle* magnetic dipole–dipole) influences that create many-body cooperative or "collective" magnetic behaviors that manifest or dominate in a clinical setting. This reality places further emphasis on the need to develop robust technology able to address the identified limitations by direct measurement *during* therapy; and, more clinically relevant physical models.

5 | STATE OF THE ART IN IMAGING WITH MIONPs: MRI AND ITS LIMITATIONS FOR MFH WITH MIONPs

To this point, we have left unaddressed the obvious question of the suitability of MRI for MFH, which is now discussed. Clinical MRI scanners measure time-dependent relaxation of proton nuclear magnetic moments in tissues exposed to a large static magnetic field $\geq$1.5 T. The contrast in anatomical MR images is produced from differences of proton relaxations arising from variations in tissue properties. MIONPs that possess a large saturation magnetization (M_s) when in a saturating magnetic field ($>\sim$0.6 T) exert a powerful damping field on nearby, tissue-based proton relaxations. This damping shortens MR T_2 relaxation time altering contrast of nearby tissues, creating hypointense features on the image. Although MIONPs were reported to have the ability to shorten MR T_2 relaxation times in the late 1970s (Ohgushi et al., 1978), they did not make their introduction as MR contrast agents until the 1980s (Dias & Lauterbur, 1986; Olsson et al., 1986; Renshaw et al., 1986). Since then, their primary clinical use has been as negative contrast agents for liver and lymph node imaging (Fortuin et al., 2018).

While MIONPs produce the highest relaxivity of MRI contrast agents known today with field-dependent T_2 relaxivities >100 mM/s, they have several drawbacks (Bulte et al., 1993; Bulte & Daldrup-Link, 2018; Bulte & Kraitchman, 2004; Fortuin et al., 2018; Ring et al., 2018). They are visible on MRI scans as nonspecific "black holes" (due to T_2^* dephasing), obscuring the underlying anatomical tissue structures. This strong "negative contrast" limits MRI applications to $<10^{-3}$ g Fe/g tissue, whereas current MFH requires at least 50-fold more MIONP (50–100 mg Fe/g tissue), far exceeding MRI saturation. Furthermore, the contrast is nonspecific as other endogenous sources of contrast may be confused with the injected MIONPs, such as air-tissue interfaces (skin surface, lung tissue, bowel content), hemorrhage (iron deposits), and/or motion and static magnetic field imperfections. Most important, it is difficult to quantify with precision the local tissue concentrations of MIONPs because they are detected indirectly through their effects on proton relaxation.

6 | MPI: AN EMERGING MODALITY

MPI is an evolving modality that exploits unique imaging physics (Gleich & Weizenecker, 2005). Unlike MRI, MPI relies on direct measurements of MIONP magnetic moments, M. Then, MIONPs are tracers for MPI as the technique sees only the MIONPs and does not see tissue. The MPI technique works by using a combination of permanent and/or electromagnets to create an intense gradient magnetic field that contains a small region of low field, that is, field free region or FFR, at their isocenter (Figure 5) (Bulte, 2019; Gleich & Weizenecker, 2005; Goodwill & Conolly, 2010, 2011). The FFR is rastered across the sample by moving the magnets or sample stage, or by varying field magnitude and directionality of electromagnets. MIONPs inside the FFR produce an MPI signal when interrogated with a low-amplitude and low-frequency AMF (e.g., 20–45 kHz), while MIONPs away from the FFR are magnetically saturated and do not produce a signal. This magnetic selection and AMF interrogation are used to produce images of the MIONP distribution throughout the subject (Gleich & Weizenecker, 2005). Importantly, the MIONP time-dependent response(s) or relaxation ($M(t) \rightarrow 0$) can provide additional information about the MIONPs and their environment, including temperature, T (see Sections 8 and 10).

Primary advantages of MPI over MRI when imaging MIONPs are its linear quantification since the MIONPs are a tracer and not a contrast agent (Bulte et al., 2015; Bulte, 2019; Gleich & Weizenecker, 2005), its theoretical higher

sensitivity of detection (depending on the MIONP), and lack of background signal conferring specificity and facilitating image interpretation. MPI also enables imaging applications in hemorrhagic tissue and air-tissue interfaces. Clinical MPI is not yet available, although a prototype device has demonstrated proof-of-principle on phantoms for brain/head imaging (Borgert et al., 2013; Graeser et al., 2019).

An inherent limitation of MPI is the lack of anatomical features, as tissue(s) are diamagnetic and produce no signal. Thus, MPI can require anatomic coregistration with X-ray CT, or MRI before injection of MIONPs. The clinical impact of this limitation is, however, manageable in modern facilities that routinely coregister multiple imaging data sets.

7 | COMBINING MPI WITH MFH: A LOGICAL NEXT EVOLUTIONARY STEP

To advance MFH combined with MPI, a key objective is to establish a clinically relevant and integrated MPI/MFH workflow in a single unit/device that incorporates MIONP-specific imaging to guide treatment planning, spatially confine the MFH within the defined target region, and control energy deposition (Figure 2). The MIONPs are simultaneously heaters and tracers, and the heat output in an AMF and spatial resolution achieved with an MPI scanner depend on the physical properties of the nanoparticles (see Sections 10 and 11). Assuming that a suitable MIONP is available, how does integrating MPI with MIONP heating advance MFH?

The unique feature of an MPI scanner's magnetic arrangement used to create the FFR for precise imaging of MIONPs also defines the region or volume of MIONP heating for MFH (Figure 5). AMFs generate heat from MIONPs by forcing rapid and repeated reversal of M (see Section 10 for discussion on physics of MIONP heating). If an AMF having suitable amplitude ($H \sim 5$ to ~ 10 kA/m) and frequency ($f \sim 100–300$ kHz) is applied to a sample within an MPI scanner, then MIONPs within the FFR will experience forced moment reversal and generate heat. MIONPs outside the FFR in the strong time-invariant MPI field are unable to generate heat for the same reason MFH cannot occur within an MRI scanner—M is at saturation and "blocked" by the strong external static field.

Heating by MIONPs exposed to an AMF occurs via hysteresis loss, which in an MPI scanner occurs only in the volume defined by the FFR therefore limiting MFH to this region. This elegant approach capitalizes on the physics of magnetic hysteresis and arrangements of (static) magnets to heat a spatially precise location within the body defined by the FFR, which also enables precise imaging of the MIONPs (Bulte, 2019; Goodwill et al., 2012; Hensley et al., 2017; Matthew et al., 2012; Tay et al., 2016, 2018).

Theoretically, MPI can accurately quantify MIONP concentration and spatial distribution within target tissue addressing another limitation of MFH (Gleich & Weizenecker, 2005; Hensley et al., 2017; Tay et al., 2018). Knowledge of MIONP distribution and location can be used to modulate AMF power (i.e., duty cycle and amplitude) with spatial control to provide a patient-specific treatment plan (Figure 2) (Attaluri et al., 2015; Ivkov et al., 2005; Kandala et al., 2019). With the appropriate modifications, it is also possible to design the MPI module to sample tissue temperature at discrete time intervals during treatment to calculate thermal dose and adjust power to ensure that energy delivery conforms to a prescribed treatment plan (see Section 8 and Figure 2).

8 | MAGNETIC NANOPARTICLE THERMOMETRY

Volumetric thermometry of the target during hyperthermia is of fundamental importance for its success. While (volumetric) MRI thermometry has become the gold standard for many thermal therapy techniques, the high static magnetic field of an MRI scanner inhibits heat generation by MIONPs and incompatible MIONP performance requirements preclude its integration with MFH (see Sections 10 and 11). Nevertheless, it has been established that MNT with MIONPs exposed to a harmonic field ($f < 5$ kHz) in the presence of a large static field as in an MRI can be obtained by tracking changes in the 4th/2nd (5th/3rd if no AMF) harmonic ratios (Rauwerdink & Weaver, 2010; Weaver et al., 2009). As MFH requires technologically compatible and non-invasive thermometry of the target during treatment, MNT within an MR scanner is impossible. To date, only MNT during MFH with MPI has demonstrated a potential to meet these criteria, particularly in the context of heterogeneous MIONP spatial distributions.

A basic principle of MNT relies on measuring time-dependent relaxation(s) of the magnetization of MIONPs, $M(t)$, after exposure to an external field. Consider a collection of *freely suspended* and *non-interacting, single-magnetic domain* MIONPs. Exposure to an external magnetic field, H, will align the sample magnetization vector or magnetic moment of

each nanoparticle, μ ($\mu = M_sV$, with M_s being the particle saturation magnetization and V the particle volume). When the field is removed ($H = 0$), sample magnetization relaxes ($M(t) \to 0$) by a combination of MIONP motion (Brownian relaxation) and internal (intraparticle) moment reorientation about the crystal axis (Néel relaxation) (Figure 1). Both relaxation processes are temperature dependent, thus we expect that the magnetization response signal measured from a sample of MIONPs exposed to a strong magnetic field will relax in a manner determined by the sample temperature (see Section 10).

By extension, the physics supports a potential to extract temperature from time-dependent response(s) of MIONP magnetization when acted on by an AMF. However, the complexities of these responses demand a robust physical model, complete understanding of the MIONP physical and magnetic properties in biological conditions, and accurate calibration (Elrefai et al., 2019; Perreard et al., 2014; Rauwerdink & Weaver, 2010; Weaver et al., 2009; Wu et al., 2017, 2019). Much of the effort to develop MNT has focused on AMF excitations <5 kHz (possible within MR scanner), whereas MFH is typically performed at 100–300 kHz and requires hysteresis precluding MR technology. Though not yet achieved, promising results with MNT in MPI scanners that operate an AMF in the FFR with $f \sim 20$–25 kHz are described below. Brownian relaxation processes typically dominate in the low frequency range, whereas Néel processes (magnetic hysteresis) generally dominate at AMF conditions used for clinical MFH (Bender et al., 2018; Dennis & Ivkov, 2013). Non-invasive MFH thermometry is challenging (Rodrigues et al., 2020), but combining MPI with other measurements of time-dependent magnetic relaxations has attracted attention (Goodwill et al., 2011). An approach to determine the temperature during MFH exploits high frequency used for heat generation and the low frequency used for temperature determination (and particle localization). Indeed, low frequency Brownian relaxation can be analyzed to infer effects of thermal damage on the tumor, for example, by changes to spatial distributions of MIONPs, and fundamental alterations (i.e., rotational dynamics) of the time-dependent (low frequency) relaxation.

Stehning et al. (2016) suggest a multicolor MPI reconstruction approach to determine temperature. A proof-of-concept is established, but calibration procedures may prove challenging for clinical applications. Salamon et al. (2020) investigated MPI for spatial and temperature distribution determination using liver phantoms to model ablation. They began by calibrating using magnetic particle spectroscopy with excitation field at 25 kHz and harmonic determination in a temperature range from 20 to 80°C. The authors determined for the samples investigated that the ratio of MPI harmonic signal at a given temperature to the harmonic value at a reference temperature (20°C) scaled approximately linearly with temperature. Magnetic nanoparticles for imaging and thermometry, and a copper (Cu) wire for heating by eddy current loss were embedded into liver phantoms. Spatial and thermal distributions in the phantoms were validated by comparing MPI temperature estimation with infrared thermometry, resulting in deviations of the order of 1°C. However, non-physical negative temperature estimates were obtained at the boundaries of the phantom, which indicate a need to develop more complex theoretical approaches. Results obtained from preclinical studies have not yet published. In addition, the approach measured responses from MIONPs in a lower frequency regime dominated by Brownian relaxation, and they were not being simultaneously excited to generate hysteresis heating by higher frequency AMF.

To estimate heat production during MFH, Tay et al. (2018) recently demonstrated a proof-of-principle dual MPI/MFH system for in vivo mouse tumor models with MPI performed using 20 kHz, during MFH at 354 kHz. The authors did not directly measure intratumor temperature during MFH, but instead developed a theoretical approach to extract the MIONP heating (i.e., power generated) as a function of position by correlating with the point spread function using x-space MPI (Goodwill & Conolly, 2010, 2011). The model determines the dynamic magnetization from the Martsenyuk–Raikher–Shliomis equation and assumes that the Brownian relaxation (particle rotation) is responsible for heat generation during MFH (Dhavalikar & Rinaldi, 2016). It is of note that power generated by the MIONPs was determined at 354 kHz where Néel processes dominate hysteresis (Bender et al., 2018). Though interesting, the approach does not reveal directly the tissue temperature. To infer tissue temperature and thermal dose from the estimated power generated by MIONPs, one needs to solve the Pennes' bioheat equation (Pennes, 1948). Overall, this is a significant step forward, but the challenge of direct and volumetric in vivo MFH thermometry remains to be solved in future developments of integrated MPI-MFH technology.

In another approach suggested by Garaio et al. (2015), the high order harmonic phases of measured $M(t)$ were used for non-invasive thermometry during MFH. In their approach, both the magnetization and phase lag harmonics were extracted from the Fourier transform of the experimentally measured dynamic magnetization using an AC magnetometer. The authors performed experiments at distinct frequencies, field amplitudes and temperatures in colloidal samples, and following calibration with optical fibers in vitro, they were able to extract accurate estimates of temperature from the third harmonic of the phase lag. While promising, this approach requires further validation in preclinical models.

9 | CHALLENGES FOR CLINICAL TRANSLATION OF A DUAL MPI/MFH SYSTEM

To this point, we have commented on the demands of clinical hyperthermia and state of art in physics and engineering that motivate development of a clinical MPI-MFH system, with integrated MNT, device to overcome current limitations of clinical MFH. We emphasize that success of such integration depends on the inherent dependence of MPI, MNT, and MFH on energetics and time-dependence of magnetic relaxations within MIONPs (see Sections 10 and 11). In turn, the MIONPs must also be synthesized with optimal values of anisotropy energy, K, to enable both imaging and therapeutic heating at clinically acceptable AMF conditions ($f \sim 100$–300 kHz; and $H \sim 5$–10 kA/m). Constraints on clinical AMF applications arise from the inevitable consequence of the interactions between time-varying electromagnetic fields and materials: AMFs induce electric currents in electrically conductive materials, which can deposit power to produce Joule heating. The power (rate of energy) absorbed by (or dissipated in) a dielectric material (e.g., biological tissue) is defined as specific absorption rate (SAR) having units W/kg material (Cleveland et al., 1997). The magnitude of SAR in tissue depends on the properties of the field, electrical conductivity, and volume (and sometimes orientation) of the tissue being exposed to the AMF (Atkinson et al., 1984; Nyenhuis et al., 1991). Having low electric conductivity and being weakly diamagnetic, biological tissues manifest much lower SAR values than many other diamagnetic (e.g., non-ferromagnetic metals such as Cu) or dielectric materials. On the other hand, thermal tolerance of biological systems places strict limitations on AMF exposures and thermal variations (Black, 2006; Dewhirst et al., 2012; Sapareto & Dewey, 1984).

It is important to note that considering definitions of SAR adopted by regulatory agencies (Cleveland et al., 1997), use of SAR to quantify heating by ferromagnetic or ferrimagnetic (i.e., MIONPs) materials in electromagnetic fields conflicts with the established definition of SAR, and it can be confusing. Furthermore, heat generated (or dissipated) by MIONPs occurs via hysteresis loss, thus to quantify heat generated by MIONPs in tissues, and to distinguish it from induced eddy current heating in tissue, it is perhaps more appropriate to use specific loss power (SLP, W/kg MIONP or Fe). Careful attention to this distinction is also vital for regulatory approval and marketing of a clinical MFH product, as regulatory agencies require validation of device performance for both therapy (i.e., SLP) and safety (i.e., SAR). Using these terms interchangeably potentially complicates documentation of performance specifications, and their clinical use.

To heat MIONPs within the FFR of an MPI scanner, a substantial volume of the tissue must simultaneously be exposed to the AMF. Exposure of large volumes of tissue, for example, human torso, to AMFs demands innovative AMF coil design, and new approaches to MFH power control and power management. Attaluri, Jackowski, et al. (2020) proposed a modified Helmholtz coil, that is, a Maxwell coil, to ensure field homogeneity while minimizing demands on power. They have also argued that, to treat tumors located deep within the body with MFH, a homogeneous field may actually lead to lower SAR than an inhomogeneous field to achieve the same field at the target. The latter approach has been adopted for current clinical MFH (i.e., NanoTherm®) therapy, potentially limiting disease treatment to anatomically accessible locations (Attaluri, Kandala, et al., 2020). Regardless of relative benefits to using homogeneous or inhomogeneous flux density fields, it remains a challenge to minimize eddy current heating (SAR) while maintaining therapeutic MIONP heating (SLP) for clinical MFH applications.

Ivkov et al. (2005) proposed pulsed power AMF to manage off-target tissue heating. This strategy seeks to exploit active thermoregulatory responses in the subject by cycling power and adjusting ON/OFF time intervals to stimulate robust thermoregulation with sufficiently long OFF times to permit adequate heat dissipation (Black, 2006; Ivkov et al., 2005). While their demonstration in mouse models may be convincing, it is unclear whether such power regulation will be successful for clinical MFH. With MPI-enabled (volumetric) thermometry, or MNT, the future holds promise for translating sophisticated temperature-feedback controls to manage AMF power. With accurate MIONP imaging and on-board MNT, there is potential to use temperature-controlled energy deposition to compensate for heterogeneous MIONP distributions (Attaluri et al., 2015; Kandala et al., 2019; Soetaert et al., 2015).

10 | MIONPs AS TRACERS, THERMOMETERS, AND HEATERS: EXPLOITING COMPLEX PHYSICS FOR THERANOSTIC APPLICATIONS

Time-dependence of responses of MIONPs to magnetic fields is integral to MPI, MFH, and MNT. Returning to our consideration of *freely suspended* and *non-interacting single-domain* MIONPs, exposure to an external magnetic field, H,

having sufficient magnitude forces the magnetization vector or magnetic moment of each MIONP to rotate and align with the external field by traversing an internal (anisotropy) energy barrier, K, defined by attributes of the MIONPs (Figure 1; Dennis & Ivkov, 2013). One of these, magnetocrystalline anisotropy, arises from the arrangement of atoms in the nanoparticle's crystal lattice (Dennis & Ivkov, 2013). Additional contributions may arise from other MIONP properties such as shape, crystal defects, surface strain, and so on; but it is the total or sum of these contributions that dictates the time-dependent response of MIONPs to a magnetic field (Dennis & Ivkov, 2013; Dennis et al., 2015). When the field is removed ($H = 0$), the measured magnetization, M, decays with a time scale, τ that depends on characteristic features of the MIONP sample and its temperature, T (Chikazumi, 1997; Dormann et al., 1997). We note many of these anisotropy energies depend explicitly on crystal volume (see below), and thus for polydisperse samples, relaxation times can display orders-of-magnitude variation within the sample.

The particle magnetization usually follows Bloch's law

$$M(T) = M(0)\left[1 - \left(\frac{T}{T_c}\right)^{\frac{3}{2}}\right], \tag{1}$$

where $M(0)$ represents the magnetization value at 0 K (Kelvin), while T_c is the critical temperature of the material. On the other hand, Néel relaxation (rotations of magnetic moment about energy barrier within the crystal) depends exponentially on the ratio of the anisotropy to the thermal energy

$$\sigma = \frac{KV}{k_B T} \tag{2}$$

with a simplified equation given by

$$\tau_N = \tau_0 e^{\sigma} \tag{3}$$

(Coffey & Kalmykov, 2012). Additionally, the effective magnetic anisotropy (K) of MIONPs also depends on temperature. One model, Zener–Callen (Aquino et al., 2020), correlates the anisotropy temperature dependence with the magnetization as

$$K(T) = K(0)\left[1 - \left(\frac{T}{T_c}\right)^{\frac{3}{2}}\right]^{\frac{l(l+1)}{2}}, \tag{4}$$

where l is related to the anisotropy symmetry ($l = 2$ for uniaxial).

Brownian relaxation (nanoparticle rotations in suspending medium) is expressed as

$$\tau_B = \frac{3\eta V_H}{k_B T}, \tag{5}$$

where V_H is the hydrodynamic particle volume and η is the viscosity of suspending medium (Dieckhoff et al., 2016). Note that viscosity is also temperature dependent, while close to a glassy transition (T_0) it can be modeled analogous to the Néel relaxation, that is, by an exponential temperature dependence

$$\eta = \eta_0 e^{\frac{E}{k_B(T-T_0)}} \tag{6}$$

with E being some characteristic energy, as found in several glassy systems (Zhang et al., 1996). While Brownian relaxation does not depend on interparticle (particle–particle) interactions, Néel relaxation is strongly influenced by interparticle magnetic dipole–dipole interactions (Zhang et al., 1996). Thus, MIONP response signal is temperature dependent and depending on the relaxation mechanism, it can depend on the nanoparticle volume fraction (i.e.,

nanoparticle concentration determines the mean interparticle separation, which influences interparticle dipole–dipole interactions) (Figure 1).

The conditions required to achieve a response in a sample of MIONPs to a magnetic field depend explicitly on the total anisotropy energy density or magnetic anisotropy constant, K, of the collection of MIONPs, and how this energy is influenced by dipole–dipole interactions. K links M to individual MIONP crystal structures through spin–orbit coupling thus defining the energy and time scale of magnetic reorientations, or relaxation (Chikazumi, 1997; Dormann et al., 1997). Stated another way, K relates the internal energy to strength of magnetic field required to decouple M from crystal directions to permit its traversal. K is intrinsic to the nanoparticle (i.e., chemical composition, crystal structure, shape, etc.), and links the *intrinsic* time-scale (τ) of responsiveness to H and T; however, its measured value depends explicitly on T and on nanoparticle concentration, thus inextricably coupling sample temperature and sample concentration with measured time-dependent properties of the nanoparticles. In this way, passively measuring the magnitude of M shortly after MIONPs are exposed to a strong gradient field yields information about MIONP concentration in a particular location, and measuring its time-dependent decay when the field is removed yields information about the local temperature (above). This energy–temperature–time convolution also defines the properties of an AMF needed to generate heat for MFH (Dennis & Ivkov, 2013).

Application of an AMF, in which the external field polarity continuously oscillates, forces the individual magnetic moments of the nanoparticles into repeated reorientation with M following H, provided the magnitude of H is sufficient to decouple M from the crystal. MIONPs may possess sufficiently low values of K, such that thermal energy (kT) at physiological temperatures enables spontaneous moment reversal yielding *superparamagnetic* (SPM) behavior, which includes characteristically short τ ($<10^{-6}$ s) (Figure 1a). In this case, MIONPs will display exceptional responsiveness to the field, with M retracing the same path at each cycle of H (Figure 1). For larger values of K or lower temperatures, or at increasingly higher AMF frequency, f, for which the time scale approaches τ, the individual magnetic moments, and eventually individual particles, cease instantaneously rotating with the magnetic field resulting in a time-dependent lag or *hysteresis*. The lagging M, with respect to H, produces a hysteresis loop in measured M versus H (Figure 1b). The (net) work required to traverse the anisotropy energy barrier by *forced* rotation of the individual nanoparticle magnetic moments is dissipated as heat. The area of the hysteresis loop is proportional to hysteresis loss power, or amount of heat generated per AMF cycle (Dennis & Ivkov, 2013). When MIONPs are immobilized, as in biological tissues, randomized crystalline axis orientations of the individual MIONPs with respect to the external field vector produce a varied area of hysteresis loop of each MIONP with respect to the others (Aquino et al., 2020; Conde-Leboran et al., 2015; Soetaert et al., 2020). Thus, under specific conditions MIONPs generate *hysteresis loss* heating when exposed to AMFs because forced rotation of M traces an *irreversible* path through an energy barrier, producing *work* (heat) as a consequence of the first law of thermodynamics for magnetic systems (Chikazumi, 1997; Dennis & Ivkov, 2013; Soetaert et al., 2020) (Figure 1c).

11 | MIONP REQUIREMENTS FOR INTEGRATED IMAGING AND HYPERTHERMIA

MIONPs exhibiting SPM properties (i.e., *SPIO-like*—having low concentration, $<10^{-4}$ g Fe/g tissue and fast relaxation, $\tau < 10^{-6}$ s) make ideal MRI contrast agents as they do not saturate MR signal intensity and avoid creating strong signal blooming artifacts in the imaged tissues. On the other hand, for MFH MIONPs require $\tau \sim f^{-1}$ or greater, to generate sufficient hysteresis loss in a clinical MFH device, for example, $f \cong 10^5$ Hz; and, [MIONP] $\geq 10^{-3}$ g Fe/g tissue having SLP $\geq 10^5$ W/kg to generate sufficient total heating for therapy. While specific values of minimum MIONP concentration needed for clinical MFH depend on an *effective K* resulting from the colloidal state of the MIONPs in tissue, properties of the device, and on individual patient attributes; MIONPs exhibiting SPM properties at clinically relevant conditions are unsuitable for MFH (Figure 1c) (Dennis & Ivkov, 2013; Dennis et al., 2015). MIONPs exhibiting SPM properties, that is, SPIOs, at clinical MFH conditions exhibit *no* heating, as the work required to traverse the anisotropy energy barrier is explicitly zero (Figure 1b). Furthermore, MIONPs that generate measurable heat when exposed to AMFs at clinical conditions are either inherently not SPIOs (i.e., single-domain, short relaxation time, τ), or they have transitioned out of the SPM regime because the clinical AMF f is within the range of τ and/or dipole–dipole interactions are influential. Confusion describing the clinical utility of SPIOs for MFH often arises from attributes of nanoparticles measured in idealized laboratory (non-clinical) conditions, and extrapolated without the benefit of robust physical models (Figure 1) (Branquinho et al., 2013; Dennis & Ivkov, 2013; Dennis et al., 2015). The incompatible performance

specifications for MRI and MFH challenge any single MIONP formulation to perform reliably as *both* MRI and MFH theranostic agent (Dennis & Ivkov, 2013; Dennis et al., 2015).

At clinically relevant T, a large K requires a large H (>10 kA/m) to force magnetization reversal. Such MIONPs typically manifest long τ, making hysteresis possible at lower f provided H exceeds a minimum value to induce a reversal in M. MIONPs exhibiting these properties can *potentially* generate substantial heating ($\sim 10^6$ W/kg material), however, clinically appropriate AMF conditions ($H < 12$ kA/m) are typically insufficient to generate substantial hysteresis thus limiting their utility for MFH (Figure 1c). Values of K should be within specific (intermediate) limits that are matched with the clinical theranostic device to permit field-driven decoupling of M (Dennis & Ivkov, 2013; Dennis et al., 2015; Soetaert et al., 2020).

Models of MPI tracer efficiency, and incidentally on heating for MFH, are based on concepts of non-interacting SPM particles (i.e., low concentration) responding to very low-amplitude and low frequency magnetic fields (linear response theory or LRT) (Matthew et al., 2012). This is because the dilute (i.e., non-interacting) and linear response limits allow development of tractable analytical expressions to describe their properties. More recent attempts to explicitly include interparticle magnetic dipole–dipole interactions demonstrate these can introduce substantial changes to MIONP time-dependent processes critically affecting their properties for MPI and MFH (Aquino et al., 2020; Branquinho et al., 2013). A key parameter for MPI is maximum value (peak) and width of the point-spread function, defined as the derivative of M with respect to H, with narrow distribution at full width half maximum. For SPIOs (single-domain), ideal tracer properties are (directly) related to nanoparticle volume (V) or size, and size distribution (Shasha et al., 2019). On the other hand, for multi-domain or multi-core MIONPs this relationship is less developed. Recent synthesis methods have yielded MIONPs comprising aggregates of single-domain crystallites (i.e., multi-crystallite or multi-core) MIONPs having complex micro-magnetic domain structures that, interestingly, produce superior MPI signal—contrary to expectations based on models derived from SPM response and LRT (Figure 1c) (Eberbeck et al., 2013). In addition, multi-core MIONP constructs exhibiting properties intermediate between single- and multi-domain, for example, "pseudo-single domain" or "quasi-multi domain" show promise for both MPI and MFH (Basly et al., 2010; Dennis et al., 2015). It is presently unclear why these MIONPs tend to display superior tracer and heating properties, though some clues have emerged from neutron scattering experiments (Bender et al., 2018; Dennis et al., 2015, 2009).

Given the (total) anisotropy energy of a single-domain particle is, to a first approximation, proportional to V early efforts to develop MIONPs for MFH focused on synthesis of single-domain particles with controlled size and size distribution. Reliable, industrial-scale manufacturing of single-domain MIONPs having precisely controlled properties within this narrow range between magnetic single- and multi-domain has proven elusive. Thus, the alternative approach—synthesizing MIONPs via in situ controlled aggregation of magnetic iron oxide crystallites – has gained popularity (Basly et al., 2010; Dennis et al., 2015, 2009; Eberbeck et al., 2013; Gruettner et al., 2007). This method exploits the long-range nature of magnetism to create complex micromagnetic spin structures within the (aggregate) MIONP core via collective and/or exchange interactions among the aggregated single-domain crystallites (Bender et al., 2018; Dennis & Ivkov, 2013; Dennis et al., 2015). Furthermore, interparticle magnetic (dipole–dipole) interactions encountered when MIONPs are immobilized in aggregated states in tissues occur, and these interactions inevitably modify the individual MIONP properties (Branquinho et al., 2013). In other words, SPM single-domain nanoparticles that individually display negligible hysteresis at physiologically relevant conditions may produce, at high concentrations or when aggregated, a *collective* magnetization that provides remarkably useful heating for MFH (Ivkov, 2010). A key advantage of the synthesis approach used to exploit intraparticle magnetic interactions is ease and reliability to manufacture MIONPs having magnetic properties better suited for in vivo MFH, MPI, and MPI/MFH (Aquino et al., 2019, 2020; Dennis et al., 2009, 2015; Eberbeck et al., 2013; Gruettner et al., 2007; Gul et al., 2019; Habib, 2008; Hedayati et al., 2013; Hensley et al., 2017; Hoopes, Mazur, Osterberg, Song, Gladstone, Steinmetz, Veliz, Bursey, Wagner, Rajan, et al., 2017; Hoopes, Mazur, Osterberg, Song, Gladstone, Steinmetz, Veliz, Bursey, Wagner, & Fiering, 2017; Ivkov et al., 2006; Ivkov, 2010, 2019; Lanier et al., 2019; Tay et al., 2016).

To avoid confusion, we emphasize that the multi-core (multi-crystallite) MIONPs described above possess complex *intraparticle* micromagnetic structures, originating from (magnetic) collective and/or exchange interactions among the aggregated crystallites (single-domain cores) comprising the magnetic multi-core of the MIONP. Thus, they can never be categorized as SPIOs or superparamagntic particles, even though they may display SPM properties at some conditions. Furthermore, the regions (quasi-domains) of parallel spin within the MIONP multi-core may not correspond to the intercrystallite boundaries within the MIONP. That said, we recognize that

interparticle magnetic dipole–dipole interactions further modify the structure and time-dependent properties of the magnetic state of individual MIONPs in ways that can profoundly affect in vivo performance of MIONPs for MFH or MPI. Indeed, the potential for MIONP aggregation to degrade SLP and tracer quality following injection into tissues is of significant concern, although evidence indicates that the manner of these nanoparticle arrangements can influence the magnetic responses of the collection (Branquinho et al., 2013; Conde-Leboran et al., 2015; Serantes et al., 2018). It is becomingly increasingly clear that magnetic (intraparticle and interparticle) dipole–dipole interactions, often ignored in theoretical descriptions of MPI and MFH, yield *collective* magnetic associations that critically affect the time-dependent properties of MIONPs. In vivo applications that require MIONPs to be localized in tissue must anticipate the influence of collective relaxation phenomena as these are likely to be unavoidable in any clinical scenario. Indeed, we emphasize that an improved knowledge of the collective relaxations in magnetic fine particle systems is relevant to developing materials with enhanced properties for combined MFH and MPI.

12 | SUMMARY AND FUTURE PROSPECTS

In summary, magnetic nanomaterials offer theranostic potential for cancer nanomedicine because their responsiveness to magnetic fields can simultaneously enable imaging and heat-based therapy. Translating this potential into clinical application requires development of magnetic nanoparticles that, in addition to possessing robust biocompatibility, must also display values of anisotropy energy and relaxation time to enable imaging and therapeutic heating at clinically acceptable conditions, and to provide signal for thermometry within an imaging scanner. In turn, device design and engineering must fully integrate imaging, thermometry, and therapeutic heating onto a single platform. Such integration is possible, but does not yet exist. Robust physical models and appropriate nomenclature that more faithfully describe MIONP properties at clinically relevant conditions are also helpful. Hyperthermia as cancer therapy offers substantial benefits to enhance treatment response and patient quality of life providing ample motivation to develop integrated MPI-MFH-MNT technologies.

CONFLICT OF INTEREST
P.W.G. is an inventor of MPI technology and an employee of Magnetic Insight, a company that develops and manufactures MPI scanners and MPI/MFH combination devices. R.I. is an inventor of nanoparticle patents. All patents are assigned to either The Johns Hopkins University or Aduro Biosciences, Inc. R.I. is a member of the Scientific Advisory Board (SAB) of Imagion Biosystems. J.W.M.B is chair of the SAB of SuperBranche, a company that develops MIONPs. All other authors report no other conflicts of interest. Dr. Bulte is an editor of the journal and was excluded from the peer-review process and all editorial decisions related to the publication of this article.

DATA AVAILABILITY STATEMENT
Data available on request from the authors.

AUTHOR CONTRIBUTIONS
Sean Healy: Investigation (equal); writing – original draft (lead); writing – review and editing (supporting). **Andris F. Bakuzis:** Conceptualization (supporting); writing – original draft (supporting); writing – review and editing (supporting). **Patrick W. Goodwill:** Conceptualization (equal); funding acquisition (supporting); writing – original draft (supporting); writing – review and editing (supporting). **Anilchandra Attaluri:** Conceptualization (supporting); funding acquisition (supporting); writing – original draft (supporting); writing – review and editing (supporting). **Jeff W. M. Bulte:** Conceptualization (equal); funding acquisition (equal); project administration (equal); resources (equal); writing – original draft (equal); writing – review and editing (equal). **Robert Ivkov:** Conceptualization (lead); funding acquisition (equal); investigation (equal); project administration (equal); resources (equal); supervision (equal); writing – original draft (lead); writing – review and editing (lead).

ORCID

Robert Ivkov https://orcid.org/0000-0002-2930-5276

RELATED WIREs ARTICLES

Functional nanoparticles for magnetic resonance imaging
Use of magnetic fields and nanoparticles to trigger drug release and improve tumor targeting
Magnetic nanoparticle biosensors

REFERENCES

Aquino, V. R. R., Figueiredo, L. C., Coaquira, J. A. H., Sousa, M. H., & Bakuzis, A. F. (2020). Magnetic interaction and anisotropy axes arrangement in nanoparticle aggregates can enhance or reduce the effective magnetic anisotropy. *Journal of Magnetism and Magnetic Materials*, *498*, 166170.

Aquino, V. R. R., Vinícius-Araújo, M., Shrivastava, N., Sousa, M. H., Coaquira, J. A. H., & Bakuzis, A. F. (2019). Role of the fraction of blocked nanoparticles on the hyperthermia efficiency on Mn-based ferrites at clinically relevant conditions. *Journal of Physical Chemistry C*, *123*, 27725–27734.

Atkinson, W. J., Brezovich, I. A., & Chakraborty, D. P. (1984). Usable frequencies in hyperthermia with thermal seeds. *IEEE Transactions on Biomedical Engineering*, *31*(1), 70–75.

Attaluri, A., Jackowski, J., Sharma, A., Kandala, S. K., Nemkov, V., Yakey, C., DeWeese, T. L., Kumar, A., Goldstein, R. C., & Ivkov, R. (2020). Design and construction of a Maxwell-type inductor coil for magnetic nanoparticle hyperthermia. *International Journal of Hyperthermia*, *37*, 1–14.

Attaluri, A., Kandala, S. K., Wabler, M., Zhuo, H., Cornejo, C., Armour, M., Hedayati, M., Zhang, Y., DeWeese, T. L., Herman, C., & Ivkov, R. (2015). Magnetic nanoparticle hyperthermia enhances radiation therapy: A study in mouse models of human prostate cancer. *International Journal of Hyperthermia*, *31*(4), 359–374.

Attaluri, A., Kandala, S. K., Zhou, H., Wabler, M., DeWeese, T. L., & Ivkov, R. (2020). Magnetic hyperthermia for treating locally advanced unresectable and borderline resectable pancreatic cancers: The role of tumor size and eddy-current heating. *International Journal of Hyperthermia*, *37*, 108–119.

Basly, B., Felder-Flesch, D., Perriat, P., Billotey, C., Taleb, J., Pourroy, G., & Begin-Colin, S. (2010). Dendronized iron oxide nanoparticles as contrast agents for MRI. *Chemical Communications*, *46*, 985–987.

Bender, P., Fock, J., Frandsen, C., Hansen, M. F., Balceris, C., Ludwig, F., Posth, O., Wetterskog, E., Bogart, L. K., Southern, P., Szczerba, W., Zeng, L., Witte, K., Grüttner, C., Westphal, F., Honecker, D., González-Alonso, D., Barquín, L. F., & Johansson, C. (2018). Relating magnetic properties and high hyperthermia performance of iron oxide nanoflowers. *Journal of Physical Chemistry C*, *122*, 3068–3077.

Black, D. R. (2006). Thermoregulation in the presence of radio frequency fields. In F. S. Barnes & B. Greenebaum (Eds.), *Biological and medical aspects of electromagnetic fields* (3rd ed., pp. 215–226). CRC Press, Taylor & Francis Group.

Bordelon, D., Cornejo, C., Gruettner, C., DeWeese, T. L., & Ivkov, R. (2011). Magnetic nanoparticle heating efficiency reveals magneto-structural differences when characterized with a wide ranging and high amplitude alternating magnetic field. *Journal of Applied Physics*, *109*, 124904.

Borgert, J., Schmidt, J. D., Schmale, I., Bontus, C., Gleich, B., David, B., Weizenecker, J., Jockram, J., Lauruschkat, C., Mende, O., Heinrich, M., Halkola, A., Bergmann, J., Woywode, O., & Rahmer, J. (2013). Perspectives on clinical magnetic particle imaging. *Biomedizinische Technik. Biomedical Engineering*, *58*(6), 551–556.

Branquinho, L. C., Carriao, M. S., Costa, A. S., Zufelato, N., Sousa, M. H., Miotto, R., Ivkov, R., & Bakuzis, A. F. (2013). Effect of magnetic dipolar interactions on nanoparticle heating efficiency: Implications for cancer hyperthermia. *Scientific Reports*, *3*, 2887. https://doi.org/10.1038/srep02887

Bulte, J. W., & Kraitchman, D. L. (2004). Iron oxide MR contrast agents for molecular and cellular imaging. *NMR in Biomedicine*, *17*(7), 484–499.

Bulte, J. W., Vymazal, J., Brooks, R. A., Pierpaoli, C., & Frank, J. A. (1993). Frequency dependence of MR relaxation times. II. Iron oxides. *Journal of Magnetic Resonance Imaging*, *3*(4), 641–648.

Bulte, J. W. M. (2019). Superparamagnetic iron oxides as MPI tracers: A primer and review of early applications. *Advanced Drug Delivery Reviews*, *138*, 293–301.

Bulte, J. W. M., & Daldrup-Link, H. E. (2018). Clinical tracking of cell transfer and cell transplantation: Trials and tribulations. *Radiology*, *289*(3), 604–615.

Bulte, J. W. M., Walczak, P., Janowski, M., Krishnan, K. M., Arami, H., Halkola, A., Gleich, B., & Rahmer, J. (2015). Quantitative "hot-spot" imaging of transplanted stem cells using superparamagnetic tracers and magnetic particle imaging. *Tomography*, *1*, 91–97.

Chao, Y., Chen, G., Liang, C., Xu, J., Dong, Z., Han, X., Wang, C., & Liu, Z. (2019). Iron nanoparticles for low-power local magnetic hyperthermia in combination with immune checkpoint blockade for systemic antitumor therapy. *Nano Letters*, *19*, 4287–4296.

Chikazumi, S. (1997). *Physics of ferromagnetism* (2nd ed., p. 27). Oxford University Press.

Cleveland, R. F., Sylvar, D. M., & Ulcek, J. L. (1997). *Evaluating compliance with FCC guidelines for human exposure to radiofrequency electromagnetic fields*. OET Bulletin 65, Federal Communications Commission Office of Engineering & Technology, Ed. 97-01, p. 5.

Coffey, W. T., & Kalmykov, Y. P. (2012). Thermal fluctuations of magnetic nanoparticles: Fifty years after Brown. *Journal of Applied Physics*, *112*, 121301.

Cole, A. J., Yand, V. C., & David, A. E. (2011). Cancer theranostics: The rise of targeted magnetic nanoparticles. *Trends in Biotechnology*, *29*, 323–332.

Conde-Leboran, I., Serantes, D., & Baldomir, D. (2015). Orientation of the magnetization easy axes of interacting nanoparticles: Influence on the hyperthermia properties. *Journal of Magnetism and Magnetic Materials*, *380*, 321–324.

Crezee, H., van Leeuwen, C. M., Oei, A. L., Stalpers, L. J. A., Bel, A., Franken, N. A., & Kok, H. P. (2015). Thermoradiotherapy planning: Integration in routine clinical practice. *International Journal of Hyperthermia*, *32*, 41–49.

Datta, N. R., Bose, A. K., Kapoor, H. K., & Gupta, S. (1990). Head and neck cancers: Results of thermoradiotherapy versus radiotherapy. *International Journal of Hyperthermia*, *6*(3), 479–486.

Dennis, C. L., & Ivkov, R. (2013). Physics of heat generation using magnetic nanoparticles for hyperthermia. *International Journal of Hyperthermia*, *29*, 715–729.

Dennis, C. L., Jackson, A. J., Borchers, J. A., Hoopes, P. J., Strawbridge, R. R., Foreman, A. R., van Lierop, J., Grüttner, C., & Ivkov, R. (2009). Nearly complete regression of tumors via collective behavior of magnetic nanoparticles in hyperthermia. *Nanotechnology*, *20*, 395103.

Dennis, C. L., Krycka, K. L., Borchers, J. A., Desutels, R. D., van Lierop, J., Huls, N. F., Jackson, A. J., Grüttner, C., & Ivkov, R. (2015). Internal magnetic structure of nanoparticles dominates time-dependent relaxation processes in a magnetic field. *Advanced Functional Materials*, *25*, 4300–4311.

Dewhirst, M., Das, S., Stauffer, P., Craciunescu, O., Vujaskovic, Z., & Thrall, D. (2011). *Hyperthermia. Clinical radiation oncology* (3rd ed., pp. 385–403). Elsevier Health Sciences.

Dewhirst, M., Stauffer, P., Das, S., Craciunescu, O., & Vujaskovic, Z. (2021). In J. E. Tepper (Ed.), *Hyperthermia. Gunderson & Tepper's clinical radiation oncology* (5th ed., pp. 381–404). Elsevier Health Sciences.

Dewhirst, M. W., Viglianti, B. L., Lora-Michiels, M., Hanson, M., & Hoopes, P. J. (2012). Basic principles of thermal dosimetry and thermal thresholds for tissue damage from hyperthermia. *International Journal of Hyperthermia*, *28*, 509–517.

Dhavalikar, R., & Rinaldi, C. (2016). Theoretical predictions for spatially-focused heating of magnetic nanoparticles guided by magnetic particle imaging field gradients. *Journal of Magnetism and Magnetic Materials*, *419*, 267–273.

Dias, M. H. M., & Lauterbur, P. C. (1986). Ferromagnetic particles as contrast agents for magnetic resonance imaging of liver and spleen. *Magnetic Resonance in Medicine*, *3*(2), 328–330.

Dieckhoff, J., Eberbeck, D., Schilling, M., & Ludwig, F. (2016). Magnetic-field dependence of Brownian and Neel relaxation times. *Journal of Applied Physics*, *119*, 043903.

Dormann, J. L., Fiorani, D., & Tronc, E. (1997). Magnetic relaxation in fina-particle systems. In I. Prigogine & S. A. Rice (Eds.), *Advances in chemical physics* (Vol. 98, pp. 283–494). Wiley.

Eberbeck, D., Dennis, C. L., Huls, N. F., Krycka, K. L., Grüttner, C., & Westphal, F. (2013). Multicore magnetic nanoparticles for magnetic particle imaging. *IEEE Transactions on Magnetics*, *49*, 269–274.

Elrefai, A. L., Yoshida, T., & Enpuku, K. (2019). Effect of viscosity on harmonics signals of magnetic nanoparticles for thermometry applications. *Journal of Magnetism and Magnetic Materials*, *491*, 165480.

Falk, M. H., & Issels, R. D. (2001). Hyperthermia in oncology. *International Journal of Hyperthermia*, *17*, 1–18.

Fiorentini, G., Sarti, D., Gadaleta, C. D., Ballerini, M., Fiorentini, C., Garfagno, T., Ranier, G., & Guadagni, S. (2020). A narrative review of regional hyperthermia: Updates from 2010 to 2019. *Integrative Cancer Therapies*, *19*, 1–13.

Fortuin, A. S., Bruggemann, R., van der Linden, J., Panfilov, I., Israel, B., Scheenen, T. W. J., & Barentsz, J. O. (2018). Ultra-small superparamagnetic iron oxides for metastatic lymph node detection: Back on the block. *WIREs Nanomedicine and Nanobiotechnology*, *10*(1), e1471 (10 pages).

Garaio, E., Gollantes, J.-M., Garcia, J. A., Plazaola, F., & Sandre, O. (2015). Harmonic phases of the nanoparticle magnetization: An intrinsic temperature probe. *Applied Physics Letters*, *107*, 123103.

Gilchrist, R. K., Medal, R., Shorey, W. D., Hanselman, R. C., Parrott, J. C., & Taylor, C. B. (1957). Selective inductive heating of lymph nodes. *Annals of Surgery*, *146*, 596–606.

Gleich, B., & Weizenecker, J. (2005). Tomographic imaging using the nonlinear response of magnetic particles. *Nature*, *435*, 1214–1237.

Goodwill, P. W., & Conolly, S. M. (2010). The x-space formulation of the magnetic particle imaging process: One-dimensional signal, resolution, bandwidth, SNR, SAR, and magnetostimulation. *IEEE Transactions on Medical Imaging*, *29*, 1851–1859.

Goodwill, P. W., & Conolly, S. M. (2011). Multidimensional X-space magnetic particle imaging. *IEEE Transactions on Medical Imaging*, *30*, 1581–1590. https://doi.org/10.1109/TMI.2011.2125982

Goodwill, P. W., Saritas, E. U., Croft, L. R., Kim, T. N., Krishnan, K. M., Schaffer, D. V., & Conolloy, S. M. (2012). X-space MPI: Magnetic nanoparticles for safe medical imaging. *Advanced Materials*, *24*, 3870–3877.

Goodwill, P. W., Tamrazian, A., Croft, L. R., Lu, C. D., Johnson, E. M., Pidaparthi, R., Ferguson, R. M., Khandhar, A. P., Krishnan, K. M., & Conolly, S. M. (2011). Ferrohydrodynamic relaxometry for magnetic particle imaging. *Applied Physics Letters*, *98*, 262502.

Graeser, M., Thieben, F., Szwargulski, P., Werner, F., Gdaniec, N., Boberg, M., Griese, F., Möddel, M., Ludewig, P., van de Ven, D., Weber, O. M., Woywode, O., Gleich, B., & Knopp, T. (2019). Human-sized magnetic particle imaging for brain applications. *Nature Communications*, *10*, 1936 (9 pages).

Gruettner, C., Muller, K., Teller, J., Westphal, F., Foreman, A. R., & Ivkov, R. (2007). Synthesis and antibody conjugation of magnetic nanoparticles with improved specific power absorption rates for alternating magnetic field cancer therapy. *Journal of Magnetism and Magnetic Materials*, *311*, 181–186.

Gul, S., Khan, S. B., Rehman, I. U., Khan, M. A., & Khan, M. I. (2019). A comprehensive review of magnetic nanomaterials modern day theranostics. *Frontiers in Materials*, *6*, 179 (15 pages).

Habib, A. H. (2008). Evaluation of iron cobalt/ferrite core–shell nanoparticles for cancer thermotherapy. *Journal of Applied Physics*, *103*, 07A307.

Harima, Y., Nagata, K., Harima, K., Ostapenko, V. V., Tanaka, Y., & Sawada, S. (2009). A randomized clinical trial of radiation therapy versus thermoradiotherapy in stage IIIB cervical carcinoma. *International Journal of Hyperthermia*, *25*, 338–343.

Hedayati, M., Attaluri, A., Bordelon, D., Goh, R., Armour, M., Zhou, H., Cornejo, C., Wabler, M., Zhang, Y., DeWeese, T. L., & Ivkov, R. (2013). New iron-oxide particles for magnetic nanoparticle hyperthermia: An in-vitro and in-vivo pilot study. *Progress in Biomedical Optics and Imaging—Proceeding of SPIE*, *8584*, 858404-1 to 858404-10.

Hensley, D., Tay, Z. W., Dhavalikar, R., Zheng, B., Goodwill, P., Rinaldi, C., & Conolly, S. (2017). Combining magnetic particle imaging and magnetic fluid hyperthermia in a theranostic platform. *Physics in Medicine and Biology*, *62*, 3483–3500. https://doi.org/10.1088/1361-6560/aa5601

Hoopes, P. J., Mazur, C. M., Osterberg, B., Song, A., Gladstone, D. J., Steinmetz, N. F., Veliz, F. A., Bursey, A. A., Wagner, R. J., & Fiering, S. N. (2017). Effect of intra-tumoral magnetic nanoparticle hyperthermia and viral nanoparticle immunogenicity on primary and metastatic cancer. *Proceedings of SPIE—The International Society for Optical Engineering*, *10066*, 100660G. https://doi.org/10.1117/12.2256062

Hoopes, P. J., Mazur, C. M., Osterberg, B., Song, A., Gladstone, D. J., Steinmetz, N. F., Veliz, F. A., Bursey, A. A., Wagner, R. J., Rajan, A., Dugat, D., Crary-Burney, M., & Fiering, S. N. (2017). Hypo-fractionated radiation, magnetic nanoparticle hyperthermia and a viral immunotherapy treatment of spontaneous canine cancer. *Proceedings of SPIE—The International Society for Optical Engineering*, *10066*, 1–9. https://doi.org/10.1117/12.2256213

Issels, R., Kampmann, E., Kanaar, R., & Lindner, L. H. (2016). Hallmarks of hyperthermia in driving the future of clinical hyperthermia as targeted therapy: Translation into clinical application. *International Journal of Hyperthermia*, *32*, 89–95.

Ivkov, R. (2010). *Magnetic nanoscale compositions, and therapeutic methods related thereto*, U.S. Patent No. 7,731,648.

Ivkov, R. (2013). Magnetic nanoparticle hyperthermia: A new frontier in biology and medicine? Editor Introduction for special issue. *International Journal of Hyperthermia*, *29*, 703–705.

Ivkov, R. (2019). *Process for making iron oxide nanoparticle preparations for cancer hyperthermia*, U.S. Patent No. 10,406,228.

Ivkov, R., DeNardo, S. J., Daum, W., Foreman, A., Goldstein, R., Nemkov, V. S., & DeNardo, G. L. (2005). Application of high amplitude alternating magnetic fields for heat induction of nanoparticles localized in cancer. *Clinical Cancer Research*, *11*, 7093s–7103s.

Ivkov, R., Gruettner, C., Teller, J., & Westphal, F. (2006). *Magnetic nanoparticle compositions, and methods related thereto*, EP Patent No. 1,648,381.

Johannsen, M., Gneveckow, U., Eckelt, L., Feussner, A., Waldofner, N., Scholz, R., Deger, S., Wust, P., Loening, S. A., & Jordan, A. (2005). Clinical hyperthermia of prostate cancer using magnetic nanoparticles: Presentation of a new interstitial technique. *International Journal of Hyperthermia*, *21*, 637–647.

Johannsen, M., Gneveckow, U., Taymoorian, K., Thiesen, B., Waldofner, N., Scholz, R., Jung, K., Jordan, A., Wust, P., & Loening, S. A. (2007). Morbidity and quality of life during thermotherapy using magnetic nanoparticles in locally recurrent prostate cancer: Results of a prospective phase I trial. *International Journal of Hyperthermia*, *23*, 315–323.

Johannsen, M., Gneveckow, U., Thiesen, B., Taymoorian, K., Cho, C. H., Waldofner, N., Scholz, R., Jordan, A., Loening, S. A., & Wust, P. (2007). Thermotherapy of prostate cancer using magnetic nanoparticles: Feasibility, imaging, and three-dimensional temperature distribution. *European Urology*, *52*, 1653–1662.

Johannsen, M., Thiesen, B., Wust, P., & Jordan, A. (2010). Magnetic nanoparticle hyperthermia for prostate cancer. *International Journal of Hyperthermia*, *26*, 790–795.

Jordan, A., Scholz, R., Maier-Hauff, K., van Landeghem, F. K., Waldoefner, N., Teichgraeber, U., Pinkernelle, J., Bruhn, H., Neumann, F., Thiesen, B., von Deimling, A., & Felix, R. (2006). The effect of thermotherapy using magnetic nanoparticles on rat malignant glioma. *Journal of Neuro-Oncology*, *78*, 7–14.

Kandala, S. K., Liapi, E., Whitcomb, L. L., Attaluri, A., & Ivkov, R. (2019). Temperature-controlled power modulation compensates for heterogeneous nanoparticle distributions: A computational optimization analysis for magnetic hyperthermia. *International Journal of Hyperthermia*, *36*, 115–129.

Kok, H. P., Cressman, E., Ceelen, W. P., Brace, C., Ivkov, R., Grüll, H., ter Haar, G., Wust, P., & Crezee, H. (2020). Heating technology for malignant tumors: A review. *International Journal of Hyperthermia*, *37*, 711–741.

Korangath, P., Barnett, J. D., Sharma, A., Henderson, E. T., Stewart, J., Yu, S. H., Kandala, S. K., Yang, C. T., Caserto, J. S., Hedayati, M., Armstrong, T. D., Jaffee, E., Gruettner, C., Zhou, X. C., Fu, W., Hu, C., Sukumar, S., Simons, B. W., & Ivkov, R. (2020). Nanoparticle interactions with immune cells dominate tumor retention and induce T cell-mediated tumor suppression in models of breast cancer. *Science Advances*, *6*, eaay1601.

Kut, C., Zhang, Y., Hedayati, M., Zhou, H., Cornejo, C., Bordelon, D., Mihalic, J., Wabler, M., Burghardt, E., Gruettner, C., Geyh, A., Brayton, C., DeWeese, T. L., & Ivkov, R. (2012). Preliminary study of injury from heating systemically delivered, nontargeted dextran-superparamagnetic iron oxide nanoparticles in mice. *Nanomedicine (London, England)*, *7*, 1697–1711. https://doi.org/10.2217/nnm.12.65

Lanier, O. L., Korotych, O. I., Monsalve, A. G., Wable, D., Savliwala, S., Grooms, N. W. F., Nacea, C., Tuitt, O. R., & Dobson, J. (2019). Evaluation of magnetic nanoparticles for magnetic fluid hyperthermia. *International Journal of Hyperthermia*, 36, 686–700.

Mahmoudi, K., Bouras, A., Bozec, D., Ivkov, R., & Hadjipanayis, C. (2018). Magnetic hyperthermia therapy for the treatment of glioblastoma: A review of the therapy's history, efficacy, and application in humans. *International Journal of Hyperthermia*, 34, 1316–1328.

Maier-Hauff, K., Rothe, R., Scholz, R., Gneveckow, U., Wust, P., Thiesen, B., Feussner, A., von Deimling, A., Waldoefner, N., Felix, R., & Jordan, A. (2007). Intracranial thermotherapy using magnetic nanoparticles combined with external beam radiotherapy: Results of a feasibility study on patients with glioblastoma multiforme. *Journal of Neuro-Oncology*, 81, 53–60.

Maier-Hauff, K., Ulich, F., Nestler, D., Niehoff, H., Wust, P., Thiesen, B., Orawa, H., Budach, V., & Jordan, A. (2011). Efficacy and safety of intratumoral thermotherapy using magnetic iron-oxide nanoparticles combined with external beam radiotherapy on patients with recurrent glioblastoma multiforme. *Journal of Neuro-Oncology*, 103, 317–324.

Marchal, S., El Hor, A., Millard, M., Gillon, V., & Bezdetnaya, L. (2015). Anticancer drug delivery: An update on clinically applied nanotherapeutics. *Drugs*, 75, 1601–1611.

Markezana, A., Goldberg, S. N., Kumar, G., Zorde-Khvalevsky, E., Gourevtich, S., Rozenblum, N., Galun, E., & Ahmed, M. (2021). Incomplete thermal ablation of tumors promotes increased tumorigenesis. *International Journal of Hyperthermia*, 38, 263–272.

Matthew, R., Khandhar, A. P., & Krishnan, K. M. (2012). Tracer design for magnetic particle imaging. *Journal of Applied Physics*, 111, 07B318.

Nyenhuis, J. A., Mouchawar, G. A., Bourland, J. D., & Geddes, L. A. (1991). Energy considerations in the magnetic (eddy-current) stimulation of tissues. *IEEE Transactions on Magnetics*, 27(1), 680–687.

Oda, M., Koga, S., & Jaeta, M. (1985). Effects of total-body hyperthermia on metastases from experimental mouse tumors. *Cancer Research*, 43(3), 1039–1043.

Oei, A. L., Korangath, P., Mulka, K., Helenius, M., Coulter, J. B., Stewart, J., Velarde, E., Crezee, J., Simons, B., Stalpers, L. J. A., Kok, H. P., Gabrielson, K., Franken, N. A. P., & Ivkov, R. (2019). Enhancing the abscopal effect of radiation and immune checkpoint inhibitor therapies with magnetic nanoparticle hyperthermia in a model of metastatic breast cancer. *International Journal of Hyperthermia*, 36, 47–63.

Ohgushi, M., Nagayama, K., & Wada, A. (1978). Dextran-magnetite: A new relaxation agent and its application to T2 measurements in gel systems. *Journal of Magnetic Resonance*, 29(3), 599–561.

Olsson, M. B. E., Persson, B. R. R., Salford, L. G., & Schroder, U. (1986). Ferromagnetic particles as contrast agent in T2 NMR imaging. *Magnetic Resonance Imaging*, 4(5), 437–440.

Overgaard, J., Gonzalez Gonzalez, D., Hulshof, M. C., Arcangeli, G., Dahl, O., Mella, O., & Bentzen, S. M. (1995). Randomised trial of hyperthermia as adjuvant to radiotherapy for recurrent or metastatic malignant melanoma. European Society for Hyperthermic Oncology. *Lancet*, 345(8949), 540–543.

Pennes, H. H. (1948). Applied physiology. *Journal of Applied Physiology*, 1, 93–122.

Perreard, I. M., Reeves, D. B., Zhang, X., Kuehlert, E., Forauer, E. R., & Weaver, J. B. (2014). Temperature of the magnetic nanoparticle microenvironment: Estimation from relaxation times. *Physics in Medicine and Biology*, 59, 1109–1119.

Rauwerdink, A. M., & Weaver, J. B. (2010). Harmonic phase angle as a concentration-independent measure of nanoparticle dynamics. *Medical Physics*, 37, 2587–2592.

Renshaw, P. F., Owen, C. S., McLaughlin, A. C., Frey, T. G., & Leigh, J. S., Jr. (1986). Ferromagnetic contrast agents: A new approach. *Magnetic Resonance in Medicine*, 3(2), 217–225.

Repasky, E. A., Evans, S. S., & Dewhirst, M. W. (2013). Temperature matters! And why it should matter to tumor immunologists. *Cancer Immunology Research*, 1, 210–216.

Ring, H. L., Zhang, J., Klein, N. D., Eberly, L. E., Haynes, C. L., & Garwood, M. (2018). Establishing the overlap of IONP quantification with echo and echoless MR relaxation mapping. *Magnetic Resonance in Medicine*, 79, 1420–1428.

Rodrigues, H. F., Capistrano, G., & Bakuzis, A. F. (2020). *In vivo* magnetic nanoparticle hyperthermia: A review on preclinical studies, low-field nano-heaters, noninvasive thermometry and computer simulations for treatment planning. *International Journal of Hyperthermia*, 37, 76–99.

Salamon, J., Dieckhoff, J., Kaul, M. G., Jung, C., Adam, G., Möddel, M., Knopp, T., Draack, S., Ludwig, F., & Ittrich, H. (2020). Visualization of spatial and temporal temperature distributions with mangetic particle imaging for liver tumor ablation therapy. *Scientific Reports*, 10, 7480.

Sapareto, S. A., & Dewey, W. C. (1984). Thermal dose determination in cancer therapy. *International Journal of Radiation Oncology, Biology, Physics*, 10(6), 787–800.

Serantes, D., Chantrell, R., Gavilán, H., del Morales, M. P., Chubykalo-Fesenko, O., Baldomir, D., & Satoh, A. (2018). Anisotropic magnetic nanoparticles for biomedicine: Bridging frequency separated AC-field controlled domains of actuation. *Physical Chemistry Chemical Physics*, 20, 30445–30454.

Shasha, C., Teeman, E., & Krishnan, K. M. (2019). Nanoparticle core size optimization for magnetic particle imaging. *Biomedical Physics and Engineering Express*, 5, 055010.

Sneed, P. K., Stauffer, P. R., McDermott, M. W., Diederich, C. J., Lamborn, K. R., Prados, M. D., Chang, S., Weaver, K. A., Spry, L., Malec, M. K., Lamb, S. A., Voss, B., Davis, R. L., Wara, W. M., Larson, D. A., Phillips, T. L., & Gutin, P. H. (1998). Survival benefit of hyperthermia in a prospective randomized trial of brachytherapy boost ± hyperthermia for glioblastoma multiforme. *International Journal of Radiation Oncology, Biology, Physics*, 40(2), 287–295.

Soetaert, F., Dupré, L., Ivkov, R., & Crevecoeur, G. (2015). Computational evaluation of amplitude modulation for enhanced magnetic nano-particle hyperthermia. *Biomedizinische Technik. Biomedical Engineering*, *60*, 491–504.

Soetaert, F., Korangath, P., Serantes, D., Fiering, S., & Ivkov, R. (2020). Cancer therapy with iron oxide nanoparticles: Agents of thermal and immune therapies. *Advanced Drug Delivery Reviews*, *163-164*, 65–83.

Stehning, C., Gleich, B., & Rahmer, J. (2016). Simultaneous magnetic particle imaging (MPI) and temperature mapping using multi-color MPI. *International Journal on Magnetic Particle Imaging*, *2*, 1612001 (6 pages).

Tay, Z. W., Chandrasekharan, P., Chiu-Lam, A., Hensley, D. W., Dhavalikar, R., Zhou, X. Y., Yu, E. Y., Goodwill, P. W., Zheng, B., Rinaldi, C., & Conolly, S. M. (2018). Magnetic particle imaging-guided heating in vivo using gradient fields for arbitrary localization of magnetic hyperthermia therapy. *ACS Nano*, *12*, 3699–3713. https://doi.org/10.1021/acsnano.8b00893

Tay, Z. W., Goodwill, P. W., Hensley, D. W., Taylor, L. A., Zheng, B., & Conolly, S. M. (2016). A high-throughput, arbitrary-waveform, MPI spectrometer and relaxometer for comprehensive magnetic particle optimization and characterization. *Scientific Reports*, *6*, 34180.

Thrall, D. E., Prescott, D. M., Samulski, T. V., Rosner, G. L., Denman, D. L., Leorreta, R. L., Dodge, R..... K., Page, R. L., Cline, J. M., Lee, J., Case, B. C., Evans, S. M., Oleson, J. R., & Dewhirst, M. W. (1996). Radiation plus local hyperthermia versus radiation plus combination of local and whole-body hyperthermia in canine sarcomas. *International Journal of Radiation Oncology*, *34*(5), 1087–1096.

Toraya, S. B., Sheen, M. R., Baird, J. R., Barry, S., Demidenko, E., Turk, M. J., Hoopes, P. J., Conejo-Garcia, J., & Fiering, S. (2012). Phagocytes mediate targeting of iron oxide nanoparticles to tumors for cancer therapy. *Integrative Biology*, *5*, 159–171.

Toraya-Brown, S., & Fiering, S. (2014). Local tumour hyperthermia as immunotherapy for metastatic cancer. *International Journal of Hyperthermia*, *30*, 531–539.

van der Zee, J., Gonzalez, D. G., van Rhoon, G. C., van Diijk, J. D. P., van Putten, W. L. J., & Hart, A. A. M. (2000). Comparison of radiotherapy alone with radiotherapy plus hyperthermia in locally advanced pelvic tumours: A prospective, randomised, multicentre trial. Dutch Deep Hyperthermia Group. *Lancet*, *355*(9210), 1119–1125.

Wang, Y., Hong, W., Che, S., Zhang, Y., Meng, D., Shi, F., Su, J., Yang, Y., Ma, H., Liu, R., Gao, Y., Wang, J., Hui, B., Wang, J., Lu, J., Wang, T., Liu, Z., & Chen, H. (2020). Outcomes for hyperthermia combined with concurrent radiochemotherapy for patients with cervical cancer. *International Journal of Radiation Oncology, Biology, Physics*, *107*, 499–511.

Weaver, J. B., Rauwerdink, A. M., & Hansen, E. W. (2009). Magnetic nanoparticle temperature estimation. *Medical Physics*, *36*, 1822–1829.

Wu, K., Liu, J., Su, D., Saha, R., & Wan, J.-P. (2019). Magnetic nanoparticle relaxation dynamics-based magnetic particle spectroscopy for rapid and wash-free molecular sensing. *ACS Applied Materials and Interfaces*, *11*, 22979–22986.

Wu, K., Schliep, K., Zhang, X., Liu, J., Ma, B., & Wang, J.-P. (2017). Characterizing physical properties of superparamagnetic nanoparticles in liquid phase using Brownian relaxation. *Small*, *13*, 1604135.

Yang, C.-T., Korangath, P., Stewart, J., Hu, C., Fu, W., Gruettner, C., Beck, S. E., Lin, F.-H., & Ivkov, R. (2020). Systemically delivered antibody-labelled magnetic iron oxide nanoparticles are less toxic than plain nanoparticles when activated by alternating magnetic fields. *International Journal of Hyperthermia*, *37*, 59–71.

Yerushalmi, A. (1976). Influence on metastatic spread of whole-body or local tumor hyperthermia. *European Journal of Cancer*, *12*(6), 455–463.

Zanganeh, S., Hutter, G., Spitler, R., Lenkov, O., Mahmoudi, M., Shaw, A., Pajarinen, J. S., Nejadnik, H., Goodman, S., Moseley, M., Coussens, L. M., & Daldrup-Link, H. E. (2016). Iron oxide nanoparticles inhibit tumour growth by inducing pro-inflammatory macrophage polarization in tumour tissues. *Nature Nanotechnology*, *11*, 986–994.

Zhang, J., Boyd, C., & Luo, W. (1996). Two mechanisms and a scaling relation for dynamics in ferrofluids. *Physical Review Letters*, *77*, 390–393.